1

2

3

Response variance prediction using transient statistical energy analysis

5

6   Robin S. Langley,[1] David H. Hawes,[1*] Tore Butlin,[1] and Yuki Ishii[2]

7   *[1]Department of Engineering, University of Cambridge, Trumpington Street,*

8   *Cambridge, CB2 1PZ, UK*

9   *[2]Mitsubishi Heavy Industries, Ltd. 5-717-1, Fukahori-machi, Nagasaki, 851-0392,*

10   *Japan*

11

12   10/25/2018

13

14   Running Title: Transient statistical energy analysis variance method

15

16

17

18

19   * Corresponding author

20   Electronic mail: David.HAWES@3ds.com

21   Current address: Dassault Systèmes, Cambridge Science Park, Cambridge, CB4 0WN, UK

22

23

24

25   **Abstract**

26   Statistical Energy Analysis (SEA) is a prominent method for predicting the high frequency

27   response of complex structures under steady loading where the structure is split into subsystems

28   and the subsystem energies are calculated. Since at high frequencies, the dynamic response of

29   nominally identical structures can differ greatly, methods have been developed to predict both

30   the mean and variance of the energy in the subsystems of a system across an ensemble of

31   systems. SEA can be extended to predict the transient response of a system, either to shock or

32   time-varying inputs and is known as Transient SEA, although this formulation has so far only

33   been interested in the mean response. In this paper, a method for predicting the variance of the

34   transient response is derived by considering how an individual realisation can deviate from the

35   mean. A matrix differential equation for the covariance of the subsystem energies is derived

36   which is driven by terms representing the variability in the system. These variance terms are

37   provided by assuming that the natural frequencies in each subsystem conform to the Gaussian

38   Orthogonal Ensemble. The accuracy of the method is investigated both numerically and

39   experimentally using systems involving coupled plates and its limitations are discussed.

40

41   *Keywords:* TSEA; Transient vibration; Shock-induced vibration; SEA Variance

42

43

44

I. Introduction

The transient response of structures to either shock or time-varying loading is of considerable importance when designing systems to protect against failure or reduce noise. Transient Statistical Energy Analysis (TSEA) (see for example Lai and Soom, 1990b, 1990a; Langley et al., 2019; Lyon and DeJong, 1995; Manning and Lee, 1968; Pinnington and Lednik, 1996a, 1996b) is a popular technique used to predict the high frequency response of complex structures under these conditions and has been applied to both academic and industrial applications such as predicting the noise levels in buildings due to impulses and footsteps (Robinson and Hopkins, 2015).

Transient SEA is based on steady-state SEA which has been developed over a number of decades to predict the response of complex structures subjected to steady external loads. Steady-state SEA is most commonly employed at high frequencies where, due to the short wavelength of vibrations, traditional vibration analysis approaches such as the finite element method become undesirable. At these frequencies and wavelength-scales, an extremely detailed model with a very fine mesh is required and any imperfections in the system of comparable length-scale to the wavelength will have a significant effect on the structural response. Consequently, nominally identical structures can generate very different frequency response characteristics. The SEA method inherently circumvents these issues by splitting a structure into large regions that contain similar properties known as subsystems and concerning itself only with the average and variance of the energy in each subsystem where the average is taken both spatially over the subsystem and over an ensemble of nominally identical subsystems that encompasses all random imperfections.

In addition to the mean energy of each subsystem, it is important to quantify the spread of the energy within each system across the ensemble since any particular system drawn from the

ensemble may have subsystem energies that are very different from the ensemble average values. A preliminary method for calculating the response variance was suggested by Lyon and DeJong (1995), but a more suitable and widely adopted method was later developed by Langley and Cotoni (2004a). This built on the work by Langley and Brown (2004a, 2004b) that used the principle of universality, which states that if a system is sufficiently random then the statistical distribution of its natural frequencies is independent of how the system is randomised. Assuming, due to strong empirical evidence, see for example (Weaver, 1989), that the natural frequencies of a subsystem are governed by the Gaussian Orthogonal Ensemble (GOE) Mehta (2004) and that the modeshapes are Gaussian across the ensemble, the variance of the energy in a built-up system can be calculated by investigating how any single realisation differs from the mean (Langley and Cotoni, 2004a).

It is thought that the extension of steady-state SEA to the transient case is reasonable when the assumptions on which steady-state SEA are built are not violated. This generally requires the energy in the system to vary slowly with time compared to the time period of its oscillations and many modes to be excited. Under these conditions, the steady-state SEA coupling loss factors (CLFs) can be used for the transient analysis and have been shown to produce strong results (Hopkins and Robinson, 2013; Langley et al., 2019; Robinson and Hopkins, 2015) despite suggestions that time-varying CLFs could be more suitable, particularly at lower frequencies (Lai and Soom, 1990b).

At present, there exist well-tested SEA-based methods for calculating the mean and variance of the response of complex systems to steady loading and the mean response to transient and impulsive loading. This paper aims to derive a method for calculating the variance of the response under shock and transient external loading conditions using a similar approach to Langley and Cotoni (2004a). In what follows Section II presents a brief summary of the TSEA equations used to calculate the mean response before applying them in Section III to derive

94   equations for calculating the variance of the response. Numerical and experimental validation

95   using systems of coupled plates is then presented in Sections IV and V respectively before the

96   limitations of the method are discussed in Section VI and conclusions are made in Section VII.

97

98   **II. Summary of the TSEA mean equations**

99   In this section, a brief summary of the TSEA method for calculating the mean subsystem

100   energies is presented. The TSEA equation is based on the steady-state SEA equation derived

101   by Lyon and DeJong (1995) by considering a power balance between subsystems at each

102   frequency such that

103
$$\mathbf{P}_{\text{in}}(\omega) = \mathbf{A}(\omega)\mathbf{E}(\omega), \tag{1}$$

104   which can be written using index notation as

105
$$P_{\text{in},j} = \omega\eta_j E_j + \sum_{k=1}^{N} \omega\eta_{jk} n_j \left(\frac{E_j}{n_j} - \frac{E_k}{n_k} \right) \tag{2}$$

106   where ω is the frequency of interest, E_j, n_j, η_j and $P_{\text{in},j}$ are the ensemble average vibrational

107   energy, modal density, internal loss factor and power into subsystem j and η_{jk} is the coupling

108   loss factor between subsystems j and k. If the system is subjected to a shock or time-varying

109   external power input, a time derivative term can be included in the SEA equation representing

110   an increase or decrease of energy in the subsystems with time. However, this means the

111   subsystem energies are a function of both time and frequency. Most commonly, the TSEA

112   equation is averaged over a frequency band, $\omega_1 < \omega < \omega_2$ say, such that the energy variable

113   represents the time evolution of the ensemble average of the energy in a given band. The TSEA

114   equation is thus

$$\mathbf{P}_{\text{in}}(t) = \frac{d\mathbf{E}(t)}{dt} + \mathbf{A}\mathbf{E}(t) \tag{3}$$

116 where each term is now considered to be averaged over the frequency band. This equation is

117 used to derive the equations for predicting the variance of the subsystem energies.

118 Much previous work has addressed the conditions under which the steady state SEA equations,

119 Eq. (1), are valid, and these conditions can be expressed in terms of either modes or waves. In

120 modal terms, the modal responses of each subsystem must be uncorrelated and have

121 equipartition of energy, and they must also be uncorrelated from the modal responses of other

122 subsystems. An equivalent statement in terms of waves is that each subsystem must carry a

123 diffuse wavefield (in an ensemble sense), and the wavefields must be uncorrelated across the

124 different subsystems. These conditions are promoted by weak coupling between the

125 subsystems. Recent work on the mean TSEA, Eq. (3), has elucidated the additional conditions

126 which must be met for these equations to be valid (Langley et al., 2019). In wave terms, the

127 rate of change of energy within a subsystem must be slow compared to the time taken for a

128 wave to transit the subsystem several times, so that the subsystems can be considered to carry

129 diffuse wavefields at all times. This condition is again promoted by weak coupling between

130 the subsystems. The following section considers the variance of the response, and this requires

131 the additional assumption that the natural frequencies and mode shapes of each subsystem have

132 statistics which are governed by the Gaussian Orthogonal Ensemble. As discussed by Wright

133 and Weaver, 2010, this condition is widely applicable to structures which display a sufficient

134 degree of randomness, in the sense that random variations in the natural frequencies are greater

135 than the mean modal spacing (Kessissoglou and Lucas, 2009).

136

137

III. Derivation of the TSEA variance equations

This section derives the TSEA equations for predicting the time-varying variance of the system response based on the approach adopted by Langley and Cotoni (2004a). The TSEA equation that governs the ensemble average of the response of a system is given by Eq. (3). If a single realisation of the ensemble is considered then the mean TSEA equation is no longer applicable, but a similar equation can be written for the individual ensemble member that relates $\mathrm{d}\mathbf{E}(t)/\mathrm{d}t$, $\mathbf{E}(t)$ and $\mathbf{P}_{\mathrm{in}}(t)$ following the same approach as Langley and Cotoni (2004a) and noting that the terms can be written as second order in the excitation. The SEA matrix, the power input, and the response energy will all differ from the ensemble average values, and the resulting equation for a single realisation can be written as

$$\frac{\mathrm{d}}{\mathrm{d}t}\left[\mathbf{E}(t) + \tilde{\mathbf{E}}(t)\right] + \left[\mathbf{A} + \tilde{\mathbf{A}}\right]\left[\mathbf{E}(t) + \tilde{\mathbf{E}}(t)\right] = \mathbf{P}_{\mathrm{in}}(t) + \tilde{\mathbf{P}}_{\mathrm{in}}(t) \tag{4}$$

where a "tilde" over a variable represents the deviation from the ensemble average value. It has been shown by Langley and Cotoni (2004a) that power balance implies that the row sum of the SEA matrix must be zero, which implies (if N is the number of subsystems) that

$$\sum_{j}^{N} \tilde{A}_{jk} = 0 \qquad \Rightarrow \qquad \tilde{A}_{kk} = -\sum_{j \neq k}^{N} \tilde{A}_{jk}. \tag{5}$$

Hence the diagonal entries of the "random part" of the SEA matrix can be expressed in terms of the off-diagonal components. If Eq. (3) is subtracted from Eq. (4) then the result is

$$\frac{\mathrm{d}\tilde{\mathbf{E}}(t)}{\mathrm{d}t} + \mathbf{A}\tilde{\mathbf{E}}(t) + \tilde{\mathbf{A}}\mathbf{E}(t) + \tilde{\mathbf{A}}\tilde{\mathbf{E}}(t) = \tilde{\mathbf{P}}_{\mathrm{in}}(t), \tag{6}$$

and this equation can be rewritten using the summation convention in the form

$$\frac{\mathrm{d}\tilde{E}_j}{\mathrm{d}t} + A_{jk}\tilde{E}_k + \tilde{A}_{jk}E_k + \tilde{A}_{jk}\tilde{E}_{\mathrm{k}} = \tilde{P}_{\mathrm{in},j} \tag{7}$$

7

158 where the arguments of the various functions are omitted for ease of notation. Now Eq. (7)

159 can be multiplied by $\tilde{E}_r$ and averaged across the ensemble to yield

$$\mathrm{E}\left[\tilde{E}_r\left(\frac{d\tilde{E}_j}{dt} + A_{jk}\tilde{E}_k + \tilde{A}_{jk}E_k + \tilde{A}_{jk}\tilde{E}_k - \tilde{P}_{\mathrm{in},j}\right)\right] = 0. \tag{8}$$

161 Likewise the rth component of Eq. (6) can be multiplied by $\tilde{E}_j$ and averaged across the

162 ensemble to yield

$$\mathrm{E}\left[\tilde{E}_j\left(\frac{d\tilde{E}_r}{dt} + A_{rk}\tilde{E}_k + \tilde{A}_{rk}E_k + \tilde{A}_{rk}\tilde{E}_k - \tilde{P}_{\mathrm{in},r}\right)\right] = 0. \tag{9}$$

164 Equations (8) and (9) can be added, and on neglecting third order terms (or alternatively,

165 assuming that these terms average to zero) this yields

$$\dot{C}_{jr} = -A_{jk}C_{kr} - A_{rk}C_{kj} - E_k\left(q_r^{(jk)} + q_j^{(rk)}\right) + P_{jr} + P_{rj}, \tag{10}$$

167 where C_{kr} is the krth component of the covariance matrix of the energies, and the following

168 definitions are introduced

$$C_{kr} = \mathrm{E}[\tilde{E}_k\tilde{E}_r], \quad q_r^{(jk)} = \mathrm{E}[\tilde{A}_{jk}\tilde{E}_r], \quad P_{jr} = \mathrm{E}[\tilde{P}_{\mathrm{in},j}\tilde{E}_r]. \tag{11-13}$$

170 Equation (10) is a matrix Riccati equation, with "forcing" arising from the final four terms on

171 the right-hand side. Now a differential equation for the variables $q_r^{(jk)}$ can be derived by

172 multiplying Eq. (7) by $\tilde{A}_{nm}$ $(n \neq m)$ and taking the ensemble average to yield

$$\mathrm{E}\left[\tilde{A}_{nm}\left(\frac{d\tilde{E}_j}{dt} + A_{jk}\tilde{E}_k + \tilde{A}_{jk}E_k + \tilde{A}_{jk}\tilde{E}_k - \tilde{P}_{\mathrm{in},j}\right)\right] = 0. \tag{14}$$

174 By noting that the matrix $\tilde{A}_{nm}$ does not depend upon time, Eq. (14) can be written in the form

$$\dot{q}_j^{(nm)} = -A_{jk}q_k^{(nm)} - E_k\mathrm{E}[\tilde{A}_{jk}\tilde{A}_{nm}] + \mathrm{E}[\tilde{P}_{\mathrm{in},j}\tilde{A}_{nm}], \quad n \neq m. \tag{15}$$

176 Langley and Cotoni (2004a) have argued that, apart from the constraint imposed by Eq. (5),

177 the entries of the matrix $\tilde{A}_{nm}$ are uncorrelated, and moreover they are uncorrelated from the

178 power inputs. Equation (15) therefore yields

$$\dot{q}_j^{(nm)} = -A_{jk}q_k^{(nm)} - \delta_{jn}E_m\mathrm{Var}[\tilde{A}_{nm}] + \delta_{jm}E_m\mathrm{Var}[\tilde{A}_{nm}], \quad n \neq m \qquad (16)$$

180 where Var[..] represents the variance of its argument. Furthermore, the "diagonal" values of

181 $q_j^{(nm)}$ can be expressed in terms of the off-diagonal entries by employing Eq. (5) to yield

$$q_j^{(mm)} = -\sum_{n \neq m}^{N} q_j^{(nm)}. \qquad (17)$$

183 A differential equation for the terms P_{jr} that appear in Eq. (10) can be obtained by multiplying

184 Eq. (7) by $\tilde{P}_r$ and taking the ensemble average to give

$$\mathrm{E}\left[\tilde{P}_{\mathrm{in},r}\left(\frac{\mathrm{d}\tilde{E}_j}{\mathrm{d}t} + A_{jk}\tilde{E}_k + \tilde{A}_{jk}E_k + \tilde{A}_{jk}\tilde{E}_k - \tilde{P}_{\mathrm{in},j}\right)\right] = 0. \qquad (18)$$

186 Langley and Cotoni (2004a) have shown that the power input to different subsystems can be

187 considered to be uncorrelated, which means that Eq. (18) can be written as

$$\dot{P}_{rj} = -A_{jk}P_{rk} + \delta_{rj}\mathrm{Var}[\tilde{P}_{\mathrm{in},j}]. \qquad (19)$$

189 It is assumed here that $\tilde{P}_{\mathrm{in},r}$ is either constant or varies slowly with time such that $\dot{\tilde{P}}_{\mathrm{in},r}\tilde{E}_j \ll$

190 $\tilde{P}_{\mathrm{in},r}\dot{\tilde{E}}_j$. Equations (10), (16), (17) and (19) form a set of first order differential equations that

191 can be integrated to yield the variance of the response energy.

192 Note that P_{jr} arises from the presence of a *steady-state* power acting on the system, in addition

193 to any shock loading applied at $t = 0$. If the system is subjected only to shock loading, then

194 this can be applied as an initial condition on C_{kr} therefore all the terms relating to P_{jr} go to

195 zero, and the differential equation for these terms, Eq. (19), is not needed. If the external power

input varies slowly with time relative to the oscillations of the system, accurate results are also expected. It can be shown (by removing time derivatives in Eqs. (10), (16) and (19) and noting that Eq. (10) can be split and solved as a collection of terms plus their transpose) that with a steady-state power input the solution to the transient variance equations is identical to the solution that is calculated using the steady-state theory of Langley and Cotoni (2004a).

The "Var" terms that appear in Eqs. (16) and (19) act as source terms, and they can be evaluated using the theory based on the Gaussian Orthogonal Ensemble described by Langley and Brown (2004a, 2004b). The relative variance, denoted RelVar[..], of the power inputs is given by

$$\text{RelVar}[P_j] = \left(\frac{\alpha_j - 1}{\pi m_j B_j^2}\right)\left\{2B_j \tan^{-1} B_j - \ln\left(1 + B_j^2\right)\right\} + \frac{1}{\left(\pi m_j B_j\right)^2}\ln\left(1 + B_j^2\right). \qquad (20)$$

Here m_j is the effective modal overlap factor of subsystem j, which is given by Langley and Cotoni (2004a) as

$$m_j = \frac{1}{(\mathbf{C}^{-1})_{jj}}, \qquad (21)$$

where $\mathbf{C}$ is the conventional steady-state SEA matrix, $C_{jk} = A_{jk}n_k$. The parameter B_j in Eq. (20) is a bandwidth parameter defined by Langley and Cotoni (2004a) as

$$B = \Delta\frac{n_j}{m_j}. \qquad (22)$$

Finally, the parameter α_j depends on the nature of the applied loading, and for single point loading is found to be approximately 2.7 (Langley and Brown, 2004a).

The term $\text{Var}[\tilde{A}_{nm}]$ which appears in Eq. (16) can be evaluated by noting that for steady-state the relative variance of the matrix entry $\tilde{A}_{nm}$ is given by Langley and Cotoni (2004a) as

$$\text{RelVar}[\tilde{A}_{nm}] = \left(\frac{\alpha_{nm} - 1}{\pi m_n B_n^2}\right)\left\{2B_n \tan^{-1} B_n - \ln\left(1 + B_n^2\right)\right\} + \frac{1}{\left(\pi m_n B_n\right)^2}\ln\left(1 + B_n^2\right) \qquad (23)$$

216   where values for the parameter α_{nm} are also given in Langley and Cotoni (2004a).

217   At early times, immediately after an impulse all modes of the system are in phase and so power

218   transfer between subsystems is not a smooth function of time until the coherence between the

219   modes is lost. If it is assumed over the ensemble that the natural frequencies take a uniform

220   distribution, the instantaneous power transferred through the coupling between subsystems i

221   and j can be written

222
$$
\begin{aligned}
W_{ij}(t) &= \frac{1}{\Delta} \int_{\omega_1}^{\omega_2} W_{ij,av}(1 + \cos(2\omega t))\mathrm{d}\omega \\
&= W_{ij,av}\left(1 + \cos((\omega_1 + \omega_2)t)\,\operatorname{sinc}(\Delta t)\right)
\end{aligned}
\tag{24}
$$

223   where $W_{ij,av}$ is the average power transferred ω_1 and ω_2 are the lower and upper frequencies

224   of the frequency band and $\Delta = \omega_2 - \omega_1$. Ignoring the fast frequency oscillations at the $\omega_1 +$

225   ω_2 frequency, the variance of the power transfer and therefore the coupling loss factor matrix

226   must be amended such that Eq. (23) becomes

227
$$
\begin{aligned}
\operatorname{RelVar}\left[\tilde{A}_{nm}\right] = \left(1 + \operatorname{sinc}(\Delta t)\right)^2 \Bigg\{ &\left(\frac{\alpha_{nm} - 1}{\pi m_n B_n^2}\right)\{2B_n \tan^{-1} B_n - \ln(1 + B_n^2)\} \\
&+ \frac{1}{(\pi m_n B_n)^2}\ln(1 + B_n^2)\Bigg\}.
\end{aligned}
\tag{25}
$$

228   Provided the bandwidth is reasonably wide, the effect of this modification, enacted by the sinc

229   function, will decay after a short time.

230   By solving the mean TSEA equation, Eq. (3), the variance terms in the TSEA variance

231   equations, Eqs. (16) and (19), can be calculated from the relative variance of the power input

232   and coupling loss factors using Eqs. (20) and (25). All that remains for the TSEA variance

233   equations to be integrated and solved is an appropriate set of initial conditions.

234

235

A. The initial conditions

The initial conditions on the C_{kr}, $q_r^{(jk)}$ and P_{jr} variables are case dependent; however under impulsive loading, there will be no external excitation so $P_{jr} = 0$ and the initial energy in a subsystem will be uncorrelated to its coupling loss factor so $q_r^{jk} = 0$. The initial condition on the variance of the subsystem energies will only be nonzero for impulsively excited subsystems and can be obtained by noting that the modal impulse response function (assuming unit generalized mass) is given by

$$q_n(t) = \frac{\phi_n}{\omega_d} e^{-\beta \omega_n t} \sin(\omega_d t), \tag{26}$$

where β is the damping ratio, ω_n and ω_d are respectively the undamped and damped natural frequencies, and ϕ_n is the mode shape at the excitation point. The initial energy due to the impulse is therefore proportional to

$$X = \sum_{\omega_n \subset \Delta} \phi_n^2, \tag{27}$$

where the sum is over the number of modes in the frequency band. Equation (27) can also be written as

$$X = \sum_n \phi_n^2 Y(\omega_n, \Delta), \tag{28}$$

where the function Y is zero unless the natural frequency falls in the band, in which case the function equals unity. The variance of the sum X can be obtained from random point process theory (Mehta, 2004) which yields the result

$$\mathrm{Var}[X] = E[\phi_n^4] \int_0^\infty Y^2(\omega_n, \Delta) f_1(\omega_n) d\omega_n + E[\phi_n^2]^2 \int_0^\infty \int_0^\infty Y(\omega_n, \Delta) Y(\omega_m, \Delta) g_2(\omega_n, \omega_m) d\omega_n d\omega_m, \tag{29}$$

where f_1 is equal to the modal density of the system, and $g_2(\omega_n, \omega_m)$ is a function known as the second cluster function. The double integral which appears in Eq. (29) is very complicated, but progress can be made by noting that: (i) the first integral yields simply N, the average number of modes in the band, and (ii) when $\phi_n = 1$ the equation yields the number variance, denoted $\text{Var}[N]$, which is the variance of the number of modes in the band. It can therefore be deduced that

$$\text{Var}[X] = (\text{E}[\phi_n^4] - \text{E}[\phi_n^2]^2)N + \text{E}[\phi_n^2]^2\text{Var}[N]. \tag{30}$$

The mean value of X is simply $\text{E}[\phi_n^2]N$, and so the relative variance is given by

$$\text{RelVar}[X] = \frac{\alpha - 1}{N} + \frac{2}{(\pi N)^2}(\ln N + 2.18), \tag{31}$$

where the known result for the GOE number variance is employed (Mehta, 2004) and from (Langley and Brown, 2004a) $\alpha = \text{E}[\phi_n^4]/\text{E}[\phi_n^2]^2$ and is discussed below. The initial condition on the variance for any subsystem j that is subjected to an impulsive force, $f(t)$, is therefore

$$\text{E}[\tilde{E}_j^2] = \left\{ \frac{\alpha_j - 1}{N_j} + \frac{2}{(\pi N_j)^2}[\ln N_j + 2.18] \right\} E_j^2(0), \tag{32}$$

where $E_j(0)$ is the initial mean energy and can be calculated using the method of Langley et al., 2019.

The result of Eq. (32) assumes that the square of the modeshapes, ϕ_n^2, are uncorrelated from each other. However, depending on the specific application of the impulsive excitation, this correlation can be significant and act to reduce the initial energy variance. This poses a limitation on the applicability of Eq. (32) and is discussed further in Section VI.

13

B. Selecting a suitable bandwidth

Since any bandwidth of interest could be very wide, it can be split into smaller bandwidths, or 'sub-bands', and the variance from each can be added together. This assumes that each sub-band is sufficiently wide such that it is uncorrelated to neighbouring bands. The problem with taking a very wide bandwidth is that it averages over the frequency detail of the response and so can produce less accurate results. Sub-bands must therefore be selected that balance having a wide enough bandwidth that each sub-band is uncorrelated and a narrow enough bandwidth that significant frequency information is not lost. Empirical data for the modal statistics suggests that $\alpha \approx 2.7$ (Langley and Brown, 2004a) and using the assumption of GOE statistics, it has been suggested that interaction between approximately 18 neighbouring modes occurs (Langley and Cotoni, 2004b) hence a bandwidth including 18 modes could be a sensible choice. The effect of the sub-bandwidths is illustrated in the numerical validation of Section IV. Within each sub-band a centre frequency must be selected and it has been found that it is important to use the frequency at which the steady-state response is equal to the band-averaged response. This provides improved results over simply selecting the mean frequency of the sub-band.

IV. Numerical validation

In this section, the method of Section III for predicting the variance of the subsystem energies in an SEA system is validated via comparison with results calculated using the finite element method (FE). A finite element package is used to model plate structures and generate the stiffness and mass matrices required for subsequent modal analysis.

A. Methodology

Since SEA is generally applied to energy at high frequencies, any impulse applied can be thought to only excite within a given frequency band. Here this is applied as an impulse that

300 excites only the modes in the frequency range of interest. The contribution of each of these

301 modes is calculated for a given impulse location and the modal impulse responses are

302 superimposed to generate the total impulse response of the system. For a narrow frequency

303 range, this can provide poor results immediately after the impulse for subsystems that are not

304 directly forced since there are insufficient modes in the band to adequately cancel when

305 summed and produce zero energy far from the input.

306 In order to generate an ensemble of structures to compare to TSEA, the plates are randomised

307 by adding to each plate ten masses each of 2% of the plate mass and two springs of stiffness

308 $(250 \times 2\pi)^2 M_j$ at random locations where M_j is the mass of the jth plate. These values are

309 selected to generate sufficient statistical overlap in the subsystem natural frequencies to

310 produce GOE statistics as discussed by Kessissoglou and Lucas, 2009. The location of each

311 mass and spring is random, although it is ensured that they are not placed too close to the force

312 location.

313 The plate parameters used are for 5 mm thick Aluminium plate with Young's modulus 70 GPa,

314 density 2700 kg m^{-3}, Poisson ratio 0.33, loss factor 0.01 and with all edges pinned to allow

315 rotation, but zero displacement. Only out-of-plane modes are considered and an ensemble of

316 1000 realisations over a frequency range of 500-1500 Hz is used and is considered as a single

317 frequency band unless otherwise stated. The FE solution uses second order triangular shell

318 elements with a minimum element length of less than one sixth of the wavelength of vibration

319 at the highest frequency of interest. The TSEA solution was performed with a timestep of

320 2×10^{-4} s.

321

322

323

B. Prediction of the variance of the subsystem energies

324

325   For the system shown inset in Figure 1a, the mean and standard deviation TSEA results for

326   plates one and two are compared to FE results in Figure 1 where plate one is subjected to an

327   impulse. The system consists of two plates of areas 1.26 and 1.3 m^2 coupled via three point

328   connectors that are constrained to only move in the vertical direction and behave like 1D

329   springs of stiffness 2.5×10^6 N m^{-1}. The standard deviation is plotted instead of the variance

330   so the results can be more easily compared to the mean. The force location is varied with each

331   realisation and the CLFs are calculated analytically by modelling the connectors as springs. In

332   order to ensure that any errors in the transient variance results are due to deficiencies in the

333   method rather than errors carried over from the mean TSEA or steady-state SEA variance

334   methods, the mean TSEA results are tuned to fit the FE by modifying the CLFs and the steady-

335   state band-averaged variance from SEA is also tuned to closely match the variance from the

336   FE simulations by modifying the variance parameters.

337

338

339

340

341
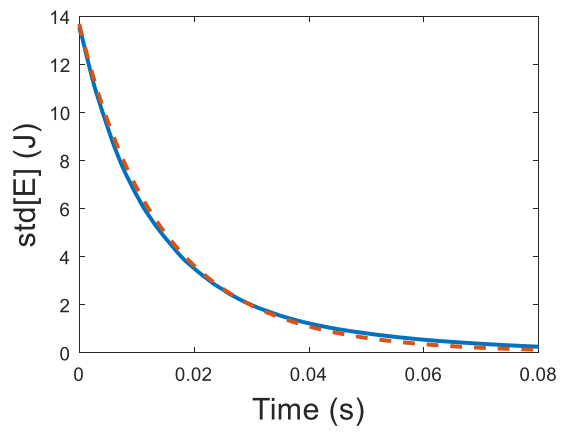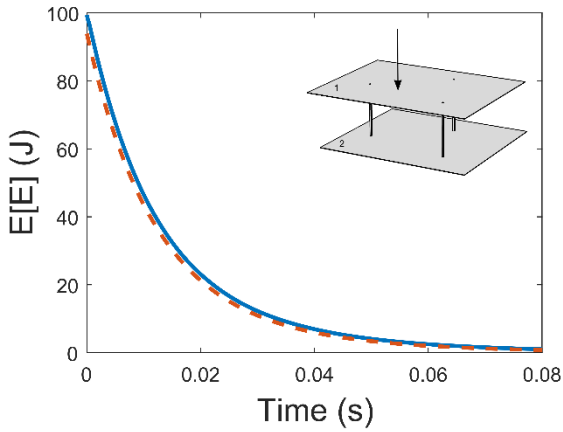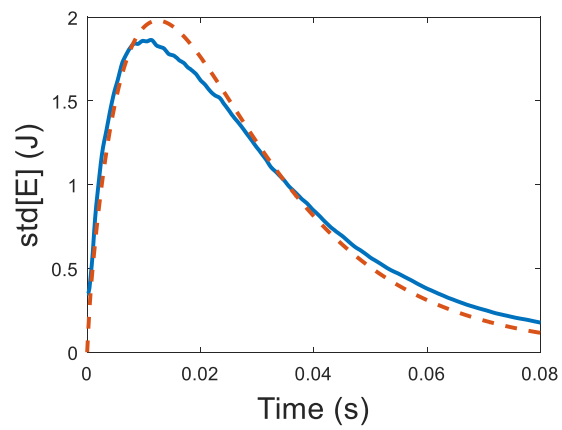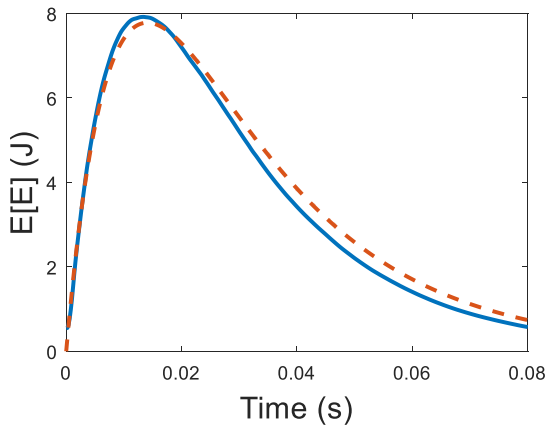
Figure 1: (Colour online) TSEA results (dashed) compared with FE results (solid) for a) plate one mean, b) plate one standard deviation, c) plate two mean and d) plate two standard deviation.

The standard deviation results show good agreement with the FE results. The variance of the initial energy in plate one is well predicted by Eq. (32) and the decay is also matched well. In plate two, the rise rate and time of maximum variance is very well predicted, with the TSEA results slightly overpredicting the maximum variance by approximately 7% and yielding a slightly slower peak time. The decay in the variance is close, but not perfectly matched to the FE results and this can be a consequence of band-averaging as discussed later.

17

356   To illustrate the necessity of calculating the variance as well as the mean of the ensemble,

357   Figure 2 presents the 95% confidence intervals for both plates, with 100 realisations of the

358   response superimposed. The variance provides an accurate measure of the spread of the

359   response and the subsystem energies of any one realisation could be under or over predicted if

360   only the mean value is used. It is assumed here that the probability density function of the

361   energy of each subsystem exhibits a lognormal distribution as discussed by Langley et al.

362   (2013). At any one time five realisations should lie outside the 95% confidence interval and

363   this is observed to be approximately true.

364

365   **a**   **b**
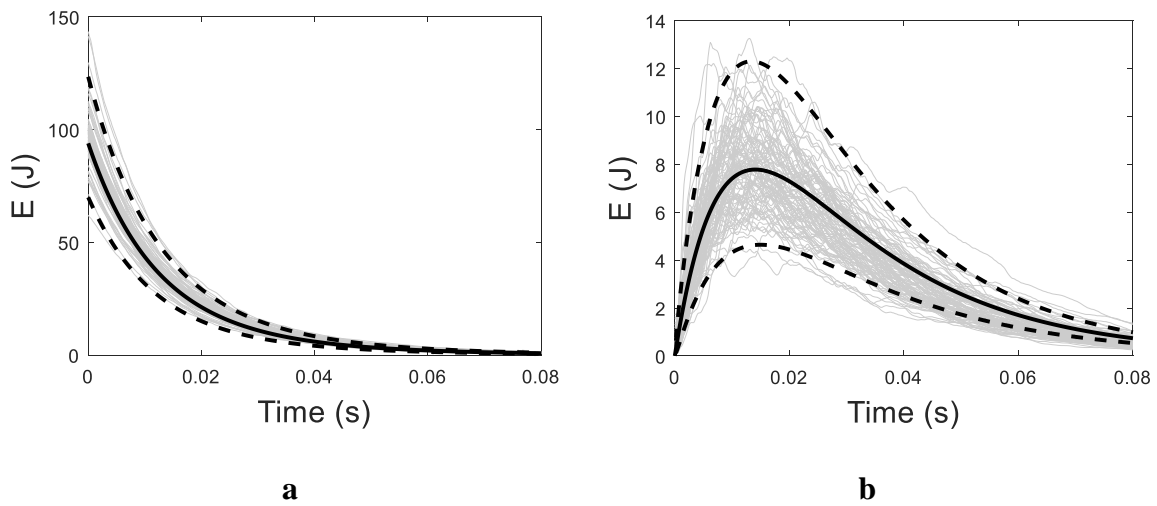
366   **Figure 2: 95% confidence interval (black dotted) from the TSEA results (mean in solid**

367   **black) compared with 100 realisations (grey), a) plate one and b) plate two.**

368

369   The effect of using different sub-bands is investigated in Figure 3 where the standard deviation

370   for both plates is plotted over the overall frequency range 500-1500 Hz with 1, 10 and 100 sub-

371   bands. The average modal density of the two plates is 0.082 modes/Hz meaning that there are

372   approximately 8 modes per 100 Hz in each subsystem. The sub-bandwidth has a noticeable

373   effect on the standard deviation, in particular the decay rate, initial conditions, peak values and

374   peak times. The initial condition in plate one is overestimated with the smallest sub-bands

375 because the assumption that bands are uncorrelated breaks down. Whilst the predictions of

376 plate two appear worse for smaller sub-bands, this is likely due to the steady-state band-

377 averaged variance being tuned for the case of a single sub-band and improving the tuning for

378 the narrower sub-bands should improve accuracy. Additionally, as the sub-bandwidth reduces,

379 the decay rate approaches that of the FE results illustrating that accuracy can decrease with a

380 wide bandwidth.
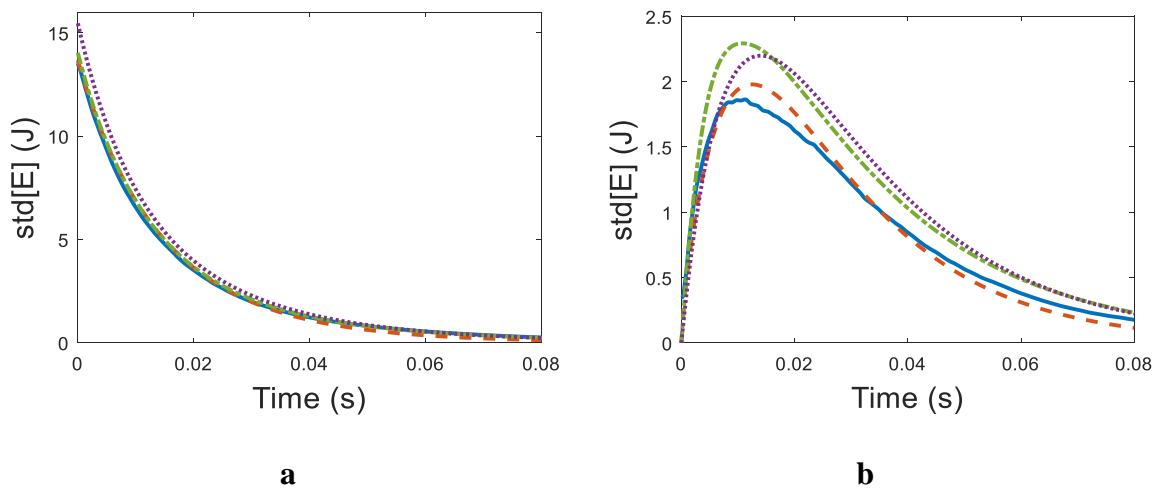
381

382 **a**   **b**

383 **Figure 3: (Colour online) Standard deviation of the energy from FE (solid) and TSEA**

384 **with 1 (dashed), 10 (dash-dot) and 100 (dotted) sub-bands for a) plate one and b) plate**

385 **two.**

386

387 It is important to discuss what level of accuracy the TSEA variance approach can be expected

388 to provide and what is considered sufficient when applied in real engineering design scenarios.

389 Due to similar assumptions in the derivation, it is reasonable to expect similar accuracy from

390 transient SEA as is achieved in steady-state SEA and therefore the two should be compared. It

391 is generally accepted that errors of ±3 dB (or approximately a factor of two) are reasonable for

392 steady-state SEA especially when considering the relative difference between subsystem

393 energies can be orders of magnitude. The predictions of the peak energy standard deviation

19

394 observed here are within 1 dB of the benchmark results. Additionally, It is most common to

395 plot SEA results on a logarithmic scale, whereas Figures 1-3 are displayed on a linear scale.

396 The results of Figure 1 are replotted on a logarithmic scale in Figure 4 where any errors now

397 look relatively small when considering the large drop in the variance of the energy between the

398 plates is well predicted. The decay rate of the variance of the energy in both plates is not

399 predicted particularly well by the TSEA and this is thought to be a feature of the band-averaging

400 as discussed above.

401

402   **a**   **b**
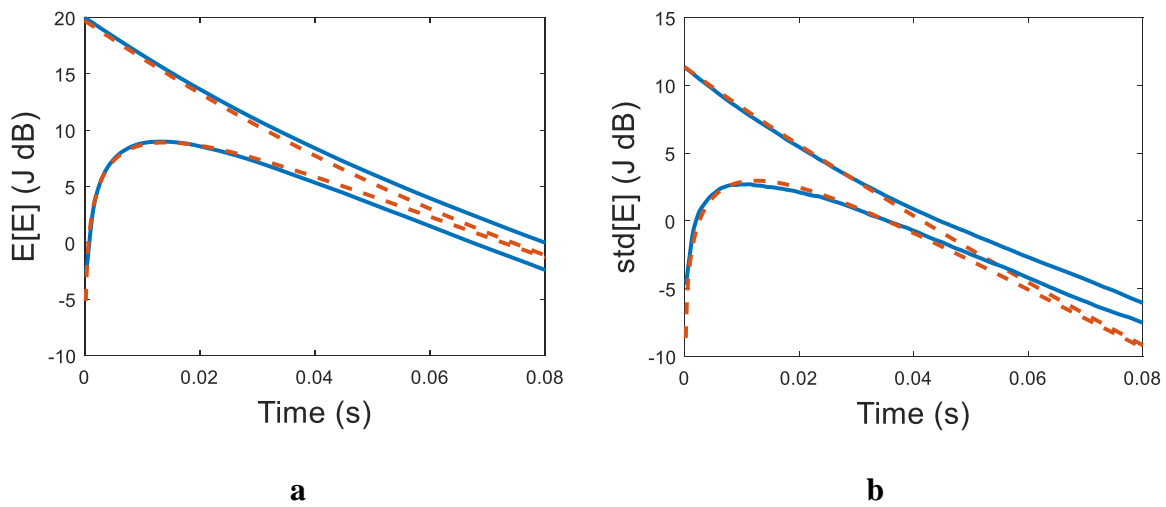
403 **Figure 4: (Colour online) a) Mean and b) standard deviation of the energy from FE**

404 **(solid) and TSEA (dashed) plotted on a logarithmic scale. Plates one and two are the top**

405 **and bottom lines respectively.**

406

407 The variance equations are also applicable when a steady-state load is applied. For the case

408 where the system used in Figure 1 is initially at rest and plate one is given a stationary band-

409 limited load with constant spectrum in the frequency range 500-1500Hz, the mean and variance

410 FE and TSEA results are shown in Figure 5. The load is applied as white noise that only acts

411 on the modes within the frequency band and the equations of motion are reformulated into the

412 non-stationary Lyapunov equation to be solved with numerical integration. In these figures,

413   horizontal lines are included to represent the results that are obtained from a purely steady-state

414   analysis and it is clear that the TSEA mean and variance results asymptote towards these values,

415   illustrating that the TSEA equations collapse to the steady-state equations under stationary

416   conditions. As before, the SEA parameters such as the CLF and input power are tuned to

417   provide close agreement with the FE results so that the transient response from the TSEA

418   method can be reasonably compared. For both the mean and standard deviation, close

419   agreement between the predicted TSEA and benchmark FE results is observed, although the

420   rise time of the standard deviation in plate one is slightly overpredicted.

421

422

423

424

425

426

427

428

429

430

431   **a**   **b**

432
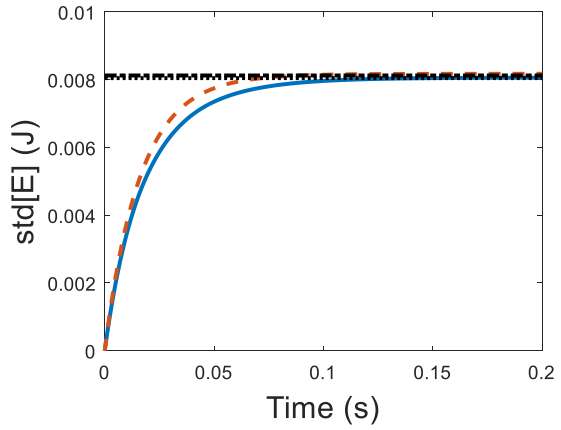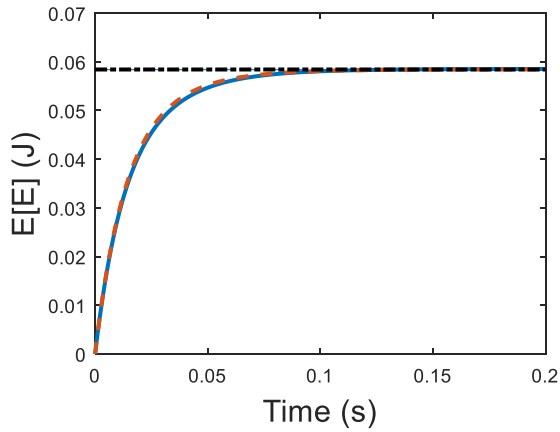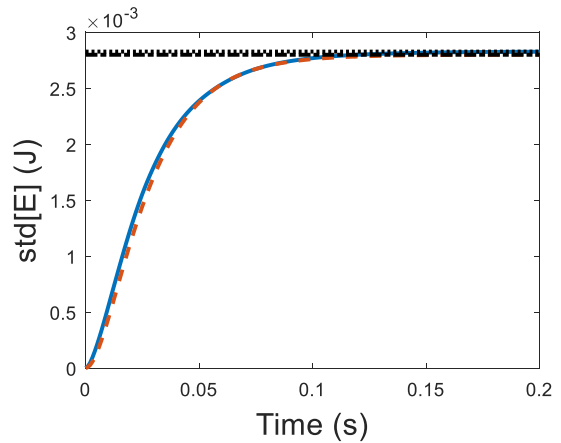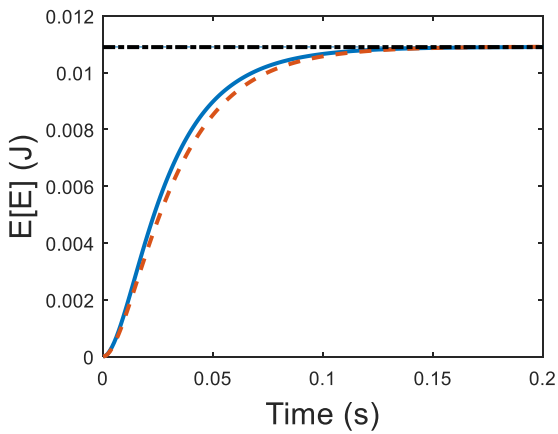
433   **c**   **d**

434 **Figure 5: (Colour online) TSEA results (dashed) compared with FE results (solid) for**

435 **plate one of the two plate system under steady loading. a) plate one mean, b) plate one**

436 **standard deviation, c) plate two mean and d) plate two standard deviation. Dash-dot**

437 **and dotted lines represent results from steady-state FE and SEA respectively.**

438

439

440

441

442

443

V. Experimental validation

To supplement the numerical validation of the TSEA method in Section IV, an experiment involving a two-plate system similar to that displayed in Figure 1 is also presented. Two aluminium plates with area 0.8 and 0.48 m^2 are suspended using string and coupled with two steel point connections as displayed inset in Figure 6a. A sharp impulse with high-frequency content is applied with a stiff-tipped impulse hammer containing a force transducer at an approximately consistent location to the upper plate, denoted plate one, and the responses of the plates are measured using five randomly spaced accelerometers on each plate from which the average velocity and therefore an estimate of the energy of each plate is calculated. In order to randomise the modeshapes and generate an ensemble of systems, a number of masses, totalling approximately 10% of the plate mass, are attached to each plate and are redistributed for each impulsive excitation.

The loss factors of each subsystem are determined at a number of frequencies by investigating the decay curves of the subsystems in isolation and are found to be approximately 0.01. The SEA coupling loss factors are then calculated from the experimental steady-state energy difference between each plate using

$$\eta_{12} = \frac{n_2 E_2}{n_2 E_1 - n_1 E_2} \eta_2 \tag{33}$$

where the modal densities are calculated analytically for a plate and η_{21} can be calculated using the reciprocity relationship $n_1 \eta_{12} = n_2 \eta_{21}$. The modal overlap factors at 1000 Hz are 1.25 and 0.75 for plates one and two respectively.

A slight extension to the variance theory of Section III must be included to account for the effect of estimating each subsystem energy from a finite number of points. This increases the observed energy variance since, in addition to the variance across the ensemble given by TSEA,

23

467   denoted $\text{Var}_{\text{ens}}(E_j)$, there is a spatial variance, denoted $\text{Var}_{\text{spa}}(E_j)$, due to spatial fluctuations

468   in energy over the subsystem at any one time. The total variance measured from the experiment

469   is therefore $\text{Var}_{\text{ens}}(E_j) + \text{Var}_{\text{spa}}(E_j)$. If there are N observation points and a realisation with

470   average energy $\overline{E}_J$ has energy at the nth point given by $E_{j,n} = \overline{E}_J + \tilde{E}_{j,n}$ then the spatial variance

471   is given by $E[\tilde{E}^2]/N$. The spatial relative variance for a system with Gaussian modeshapes is

472   unity and so the spatial variance becomes $\overline{E}^2/N$.

473   The experimental results are compared in Figure 6 to transient mean and variance results in the

474   frequency range 2000-3000 Hz where 30 realisations are taken, and the data is normalised such

475   that the peak force of each impulse is 1 N. The similarity between the two is very strong, with

476   comparable rise and decay times, although the TSEA slightly underestimates the peak standard

477   deviation in plate two. Similar to the mean results, oscillations are observed in the standard

478   deviation and would be reduced by a larger ensemble or more accelerometers as discussed in

479   Langley et al., 2019.
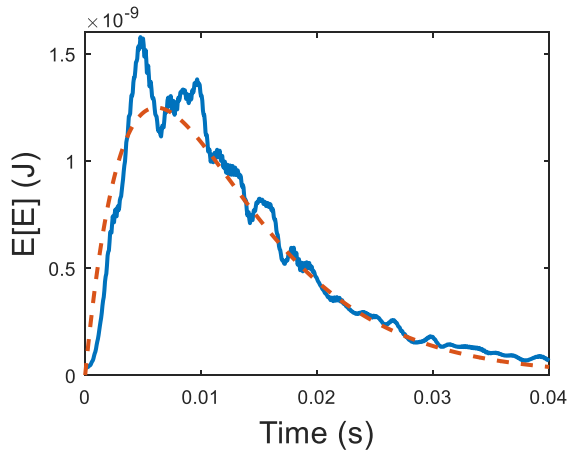
480

481

482

483

484

485

a

b

c

d
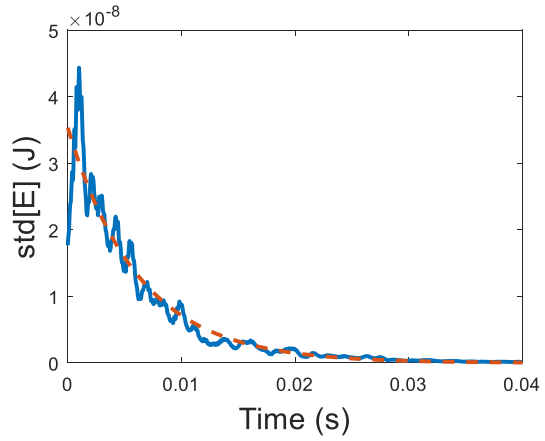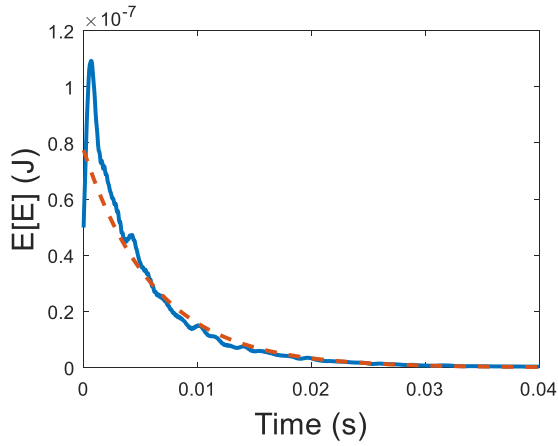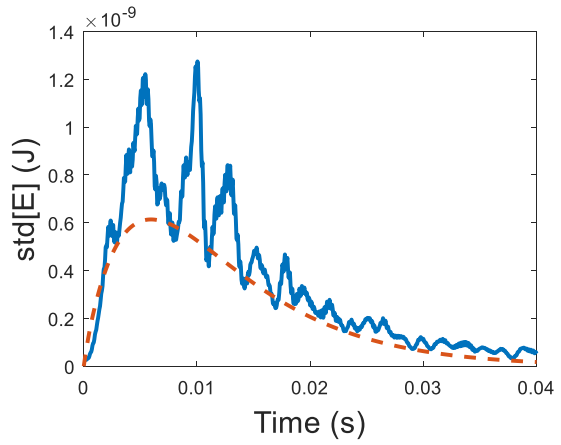
Figure 6: (Colour online) TSEA results (dashed) compared with experimental results (solid) for a) plate one mean, b) plate one standard deviation, c) plate two mean and d) plate two standard deviation.

VI. Limitations of the method

For the cases presented in Sections IV and V, the variance predictions from the derived method exhibit strong agreement with the benchmark results. However, the method is limited by the assumptions it makes thus for certain systems and loading conditions, the predictions are less accurate. These limitations are explored in this section.

499   The results of Figure 1 are obtained by varying the impulse location with each realisation. In

500   this case, the variance of the initial energy in the excited plate is reasonably predicted by Eq.

501   (32), although in fact this will generally be an overprediction since it ignores the effect of any

502   correlations between modeshapes. In the arguably more realistic case where the impulse

503   location is fixed throughout the ensemble, the effects of the correlations become greater, acting

504   to reduce the initial variance and so Eq. (32) overpredicts by an amount dependent on the

505   bandwidth of interest. This effect is displayed in Figure 7 where the impulse location is fixed

506   and the overprediction can be seen in both plates and the impact of selecting the initial variance

507   to match the FE results is shown by the dash-dot curve, which displays good accuracy. It might

508   be suggested that the correlations can be predicted by the GOE correlations (Brody et al., 1981),

509   although this has been found to be an overestimate. Should an accurate model of these

510   modeshape correlations be derived, the derived theory is expected to exhibit strong accuracy

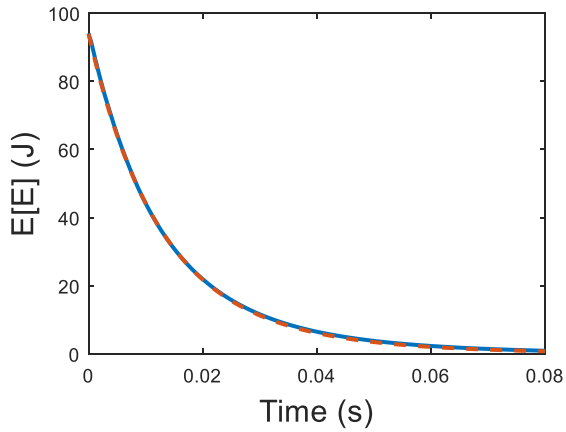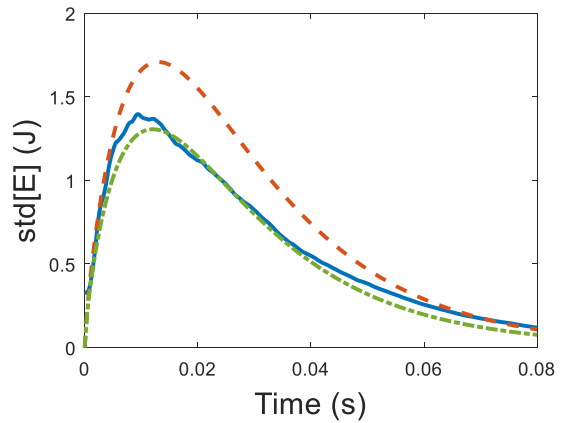511   as suggested by the dash-dot curve in Figure 7.
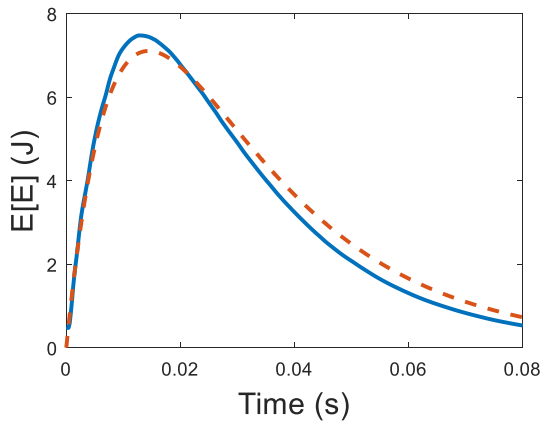
512

513

514

515

516
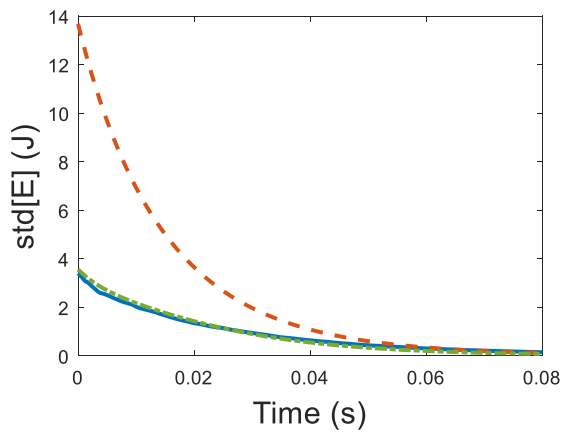
Figure 7: (Colour online) TSEA results (dashed) compared with FE results (solid) for the point coupled system when the impulse location is constant. The dash-dot curve displays the TSEA results when the initial variance in plate one is selected to match the initial variance found in the FE results. a) plate one mean, b) plate one standard deviation, c) plate two mean and d) plate two standard deviation.

A second limitation to the method is illustrated clearly by the results from the two edge-coupled plates displayed in Figure 8 where the impulse location is varied randomly with each realisation. A clear early peak in the standard deviation in the second plate is observed in the FE results in Figure 8d, but not the theoretical results. Physically, this is due to waves spreading

27

531 out from the different impulse locations of each realisation taking different amounts of time to

532 reach the edge coupling and start transferring energy through to the second subsystem.
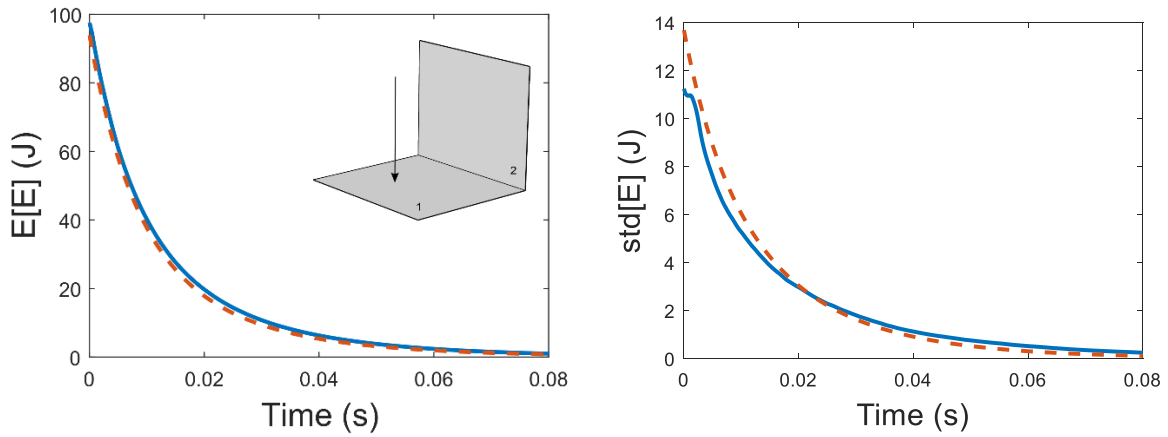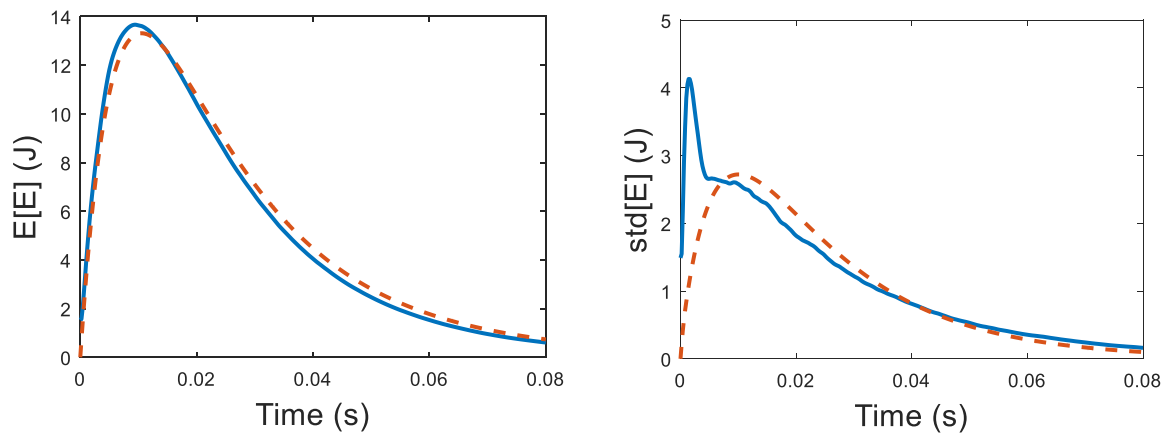
533

534 **a**   **b**

535

536 **c**   **d**

537 **Figure 8: (Colour online) TSEA results (dashed) compared with FE results (solid) for**

538 **the edge-coupled system with a varying impulse location. a) plate one mean, b) plate one**

539 **standard deviation, c) plate two mean and d) plate two standard deviation.**

540

541 The discrepancy between the theory and simulations in Figure 8d is due to the theory being

542 unable to account for the actual method of energy transfer. In Eq. (16), the variance from the

543 coupling between plates assumes a diffuse wavefield in both plates when in reality, shortly

544 after an impulse, the wavefield is a propagating wavefield and a wavefront can approach the

545   junction and cause high instantaneous transmission. It is interesting to note that this effect

546   averages out and the mean energy is unaffected. In this case, the variance prediction at later

547   times may be unreliable due to cumulative effects from the poor prediction at early times.

548   The accuracy of the method can be estimated by comparing the timescales involved in energy

549   transport. If the timescale for a subsystem to achieve a diffuse wavefield after an impulse is

550   short compared to the timescale of energy transfer between subsystems, then the derived TSEA

551   variance method can be expected to give a good prediction. This occurs when the coupling is

552   weak and explains the strong accuracy of the results of Figure 1 where the coupling is weaker.

553   Additionally, if the damping is low then energy transfer between subsystems occurs over a

554   longer time and so is greater, since the energy decay in the excited subsystem will take longer.

555   Any effect from the non-diffuse field at early times will therefore be less significant.

556   Weak coupling and low damping are well-known criteria for the reasonable application of

557   steady-state SEA. In fact, it has been suggested that a measure of coupling strength and validity

558   of SEA can be taken from mean time-domain energy plots such as Figure 8c by taking the ratio

559   of peak time to total time duration (Fahy, 1996; James and Fahy, 1997). A value of coupling

560   strength indicator of 0.07 is suggested as a reasonable threshold above which the coupling can

561   be considered weak in an SEA sense. From Figure 8c, the edge coupled system is found to

562   have a coupling strength indicator of 0.15, well above the threshold, although the variance still

563   displays a discrepancy with theory. It is therefore suggested that for reasonable application of

564   the TSEA variance method, weaker coupling is required than for steady-state SEA. It should

565   be noted that despite this limitation, the accuracy of the method is still very strong and well

566   within the expected accuracy of SEA-based approaches.

567   To investigate the effect of the wave field in the impulsively excited plate, fifty simultaneous

568   impulses are applied at random locations with zero mean and unity standard deviation Gaussian

29

569   random magnitudes with the intention of instantaneously generating a more diffuse field in the

570   plate. The results are presented in Figure 9 where the strong peak in the standard deviation of

571   the second plate is removed and the TSEA variance method provides accurate predictions. This

572   reinforces the above discussion suggesting that the method is limited by the diffuse field

573   assumption. In this case, the initial energy variance in the excited plate is matched to the FE

574   results rather than found analytically.

575

576   a   b

577

578   c   d
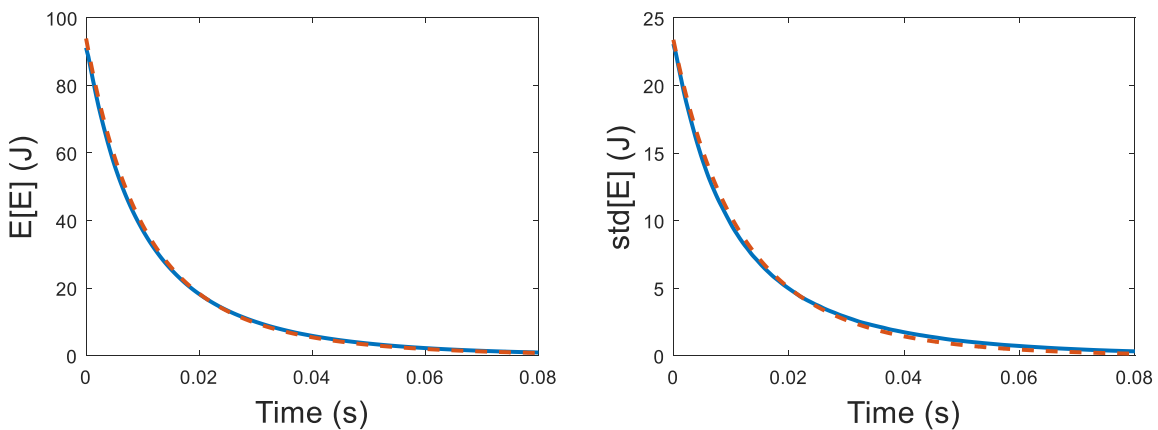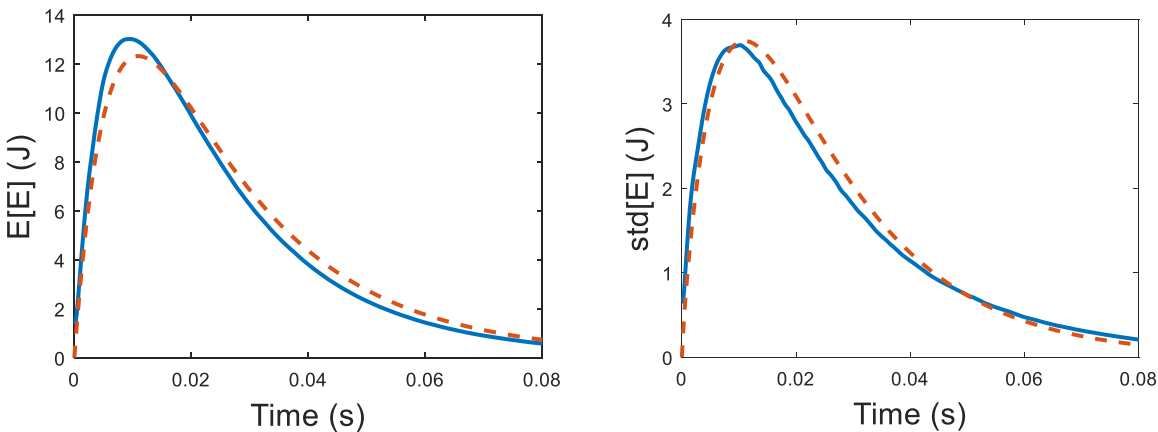
579   **Figure 9: (Colour online) TSEA results (dashed) compared with FE results (solid) for**

580   **the edge coupled system with 50 simultaneous random impulses. a) plate one mean, b)**

581   **plate one standard deviation, c) plate two mean and d) plate two standard deviation.**

582

30

VII.   Conclusions

The transient SEA method is extended to predict the variance of the energy in each subsystem of a built-up system under both impulsive and steady loads. Prediction of both the mean and the variance of a system response is important since at high frequencies, nominally identical structures can behave differently, and some measure of this variability is important when designing a structure.

Following a similar procedure to Langley and Cotoni (2004a), a power balance equation for each individual realisation of a system is manipulated to generate a differential equation for the covariance of the subsystem energies, Eq. (10). Since the variance in the response arises from variability in coupling loss factors and input power, the covariance equation is 'forced' by terms related to these variance quantities, Eqs. (16) and (19). The variance forcing terms are themselves calculated from differential equations where any variance terms are found from the ensemble statistics of the system (Langley and Brown, 2004a, 2004b). When impulsive excitation is applied, the variability across the ensemble of the energy injected into the system is imposed as an initial condition on the energy covariance matrix. Under steady-state loading, the method is shown to collapse to the steady-state SEA variance method of Langley and Cotoni (2004a).

The applicability and limitations of the derived method are investigated both numerically and experimentally and it is found to provide close agreement with benchmark results in cases of weak coupling. However, when coupling is stronger, the theoretical predictions can become less accurate due to the assumption of a diffuse field occurring instantaneously in an impulsively excited subsystem becoming less reasonable. Additionally, the variance of the initial energy in a subsystem that provides the initial condition for the covariance equation cannot yet be calculated accurately when a constant impulse location is used due to correlations

607 between modeshapes. This is a complex issue and outside of the scope of this paper, but it

608 should be noted that if the force location is not held constant, the correlations become less

609 significant and a reasonable initial condition can be applied. Despite these limitations, strong

610 results are observed and errors generally lie well within the accuracy expected from SEA-based

611 methods.

612

613 **Acknowledgements**

615

616 **References**

617 Brody, T. A., Flores, J., French, J. B., Mello, P. A., Pandey, A., and Wong, S. S. M. (**1981**).

618   "Random-matrix physics: Spectrum and strength fluctuations," Rev. Mod. Phys., **53**,

619   385–479.

620 Fahy, F. (**1996**). "A study of the kinetic energy impulse response as an indicator of the

621   strength of coupling between SEA subsystems," J. Sound Vib., **190**, 363–386.

622 Hopkins, C., and Robinson, M. (**2013**). "On the evaluation of decay curves to determine

623   structural reverberation times for building elements," Acta Acust. united with Acust., **99**,

624   226–244.

625 James, P. P., and Fahy, F. J. (**1997**). "A technique for the assessment of strength of coupling

626   between sea subsystems: Experiments with two coupled plates and two coupled rooms,"

627   J. Sound Vib., **203**, 265–282.

628 Kessissoglou, N. J., and Lucas, G. I. (**2009**). "Gaussian orthogonal ensemble spacing

629 statistics and the statistical overlap factor applied to dynamic systems," J. Sound Vib.,

630 **324**, 1039–1066.

631 Lai, M. L., and Soom, A. (**1990**). "Statistical energy analysis for the time-integrated transient

632 response of vibrating systems," J. Vib. Acoust., **112**, 206–213.

633 Lai, M. L., and Soom, A. (**1990**). "Prediction of transient vibration envelopes using statistical

634 energy analysis techniques," J. Vib. Acoust., **112**, 127–137.

635 Langley, R. S., and Brown, A. W. M. (**2004**). "The ensemble statistics of the energy of a

636 random system subjected to harmonic excitation," J. Sound Vib., **275**, 823–846.

637 Langley, R. S., and Brown, A. W. M. (**2004**). "The ensemble statistics of the band-averaged

638 energy of a random system," J. Sound Vib., **275**, 847–857.

639 Langley, R. S., and Cotoni, V. (**2004**). "Response variance prediction in the statistical energy

640 analysis of built-up systems," J. Acoust. Soc. Am., **115**, 706–718.

641 Langley, R. S., and Cotoni, V. (**2004**). "The ensemble statistics of the energy of a random

642 system subjected to harmonic excitation," J. Sound Vib., **275**, 823–846.

643 Langley, R. S., Hawes, D. H., Butlin, T., and Ishii, Y. (**2019**). "A derivation of the Transient

644 Statistical Energy Analysis (TSEA) equations with benchmark applications to plate

645 systems," J. Sound Vib. "In Press".

646 Langley, R. S., Legault, J., Woodhouse, J., and Reynders, E. (**2013**). "On the applicability of

647 the lognormal distribution in random dynamical systems," J. Sound Vib., **332**, 3289–

648 3302.

649 Lyon, R. H., and DeJong, R. G. (**1995**). *Theory and application of statistical energy analysis*,

650 Butterworth-Heinemann, Boston, 1-277 pages.

651   Manning, J. E., and Lee, K. (**1968**). "Predicting mechanical shock transmission," Shock Vib.

652   Bull., **37**, 65–70.

653   Mehta, M. L. (**2004**). *Random matrices*, Elsevier Science, San Diego, 1-706 pages.

654   Pinnington, R. J., and Lednik, D. (**1996**). "Transient energy flow between two coupled

655   beams," J. Sound Vib., **189**, 265–287.

656   Pinnington, R., and Lednik, D. (**1996**). "Transient statistical energy analysis of an

657   impulsively excited two oscillator system," J. Sound Vib., **189**, 249–264.

658   Robinson, M., and Hopkins, C. (**2015**). "Prediction of maximum fast time-weighted sound

659   pressure levels due to transient excitation from the rubber ball and human footsteps,"

660   Build. Environ., **94**, 810–820.

661   Weaver, R. L. (**1989**). "Spectral statistics in elastodynamics," J. Acoust. Soc. Am., **85**, 1005–

662   1013.

663   Wright, M., and Weaver, R. (**2010**). *New directions in linear acoustics and vibration:*

664   *Quantum chaos, random matrix theory, and complexity*, Cambridge University Press,

665   New York, pp. 42-58.

666

667

668

669

670

671

672

698 found in the FE results. a) plate one mean, b) plate one standard deviation, c) plate two mean

699 and d) plate two standard deviation.

700

701 Figure 8: TSEA results (dashed) compared with FE results (solid) for the edge-coupled

702 system with a varying impulse location. a) plate one mean, b) plate one standard deviation, c)

703 plate two mean and d) plate two standard deviation.

704

705 Figure 9: TSEA results (dashed) compared with FE results (solid) for the edge coupled

706 system with 50 simultaneous random impulses. a) plate one mean, b) plate one standard

707 deviation, c) plate two mean and d) plate two standard deviation.